Characterization of the aggregates formed by various bacterial lipopolysaccharides in solution and upon interaction with antimicrobial peptides.

Gianluca Bello,*,† Jonny Eriksson,‡ Ann Terry,¶ Katarina Edwards,‡ M. Jayne Lawrence,† David Barlow,† and Richard D. Harvey*,†

Institute of Pharmaceutical Science, King's College London, London, UK, Department of Chemistry - BMC, Uppsala University, Uppsala, Sweden, and Rutherford Appleton Laboratory, Harwell, Oxford, UK

E-mail: gianluca-bello@libero.it; richard.d.harvey@kcl.ac.uk

Phone: +44 (0)207 848 4831. Fax: +44 (0)207 848 4800

Abstract

The biophysical analysis of the aggregates formed by different chemotypes of bacterial lipopolysaccharides (LPS) before and after challenge by two different anti-endotoxic antimicrobial peptides (LL37 and bovine lactoferricin), was performed in order to determine their effect on the morphology of LPS aggregates. Small-angle neutron scattering (SANS) and cryogenic transmission electron microscopy (cryoTEM) were used to examine the structures formed by both smooth and rough LPS chemotypes and the effect of the peptides, by visualization of the aggregates and analysis of the scattering data

*To whom correspondence should be addressed
†Institute of Pharmaceutical Science, King's College London, London, United Kingdom
‡Department of Chemistry - BMC, Uppsala University, Uppsala, Sweden
¶Rutherford Appleton Laboratory, Harwell, Oxford, United Kingdom

by means of both mathematical approximations and defined models. The data showed that the structure of LPS determines the morphology of the aggregates and influences the binding activity of both peptides. The morphologies of the worm-like micellar aggregates formed by the smooth LPS were relatively unaltered by the presence of the peptides due to their pre-existing high degree of positive curvature being little affected by their association with either peptide. On the other hand the aggregates formed by the rough LPS chemotypes, showed marked morphological changes from lamellar structures to ordered micellar networks, induced by the increase in positive curvature engendered upon association with the peptides. The combined use of cryoTEM and SANS proved to be a very useful tool for studying the aggregation properties of LPS in solution at biologically relevant concentrations.

Introduction

Lipopolysaccharide (LPS) is a major component of the outer membrane (OM) of Gram negative bacteria and it is a potent stimulator of the human immune system, sometimes resulting in an uncontrolled inflammatory reaction which can worsen into severe septic shock syndrome.[1,2] The biological activity of LPS is attributed to its hydrophobic, membrane-anchoring lipid-A moiety (Figure 1), highly conserved amongst most Gram negative bacteria,[3] which is considered to be the endotoxic principle.[4] In addition to their specific lipid-A moieties, different bacterial strains can express a diverse range of LPS structures designated as either smooth or rough chemotypes, according to the presence or absence of O-antigen and the length of their core oligosaccharide, the latter often possessing lateral substituents such as ethanolamine and phosphate groups (Figure 1).[3] The inflammatory activity of LPS is thought to be mediated through the formation of aggregates, which develop in solution due to the amphiphilic nature of the LPS molecules.[5]

X-ray diffraction measurements on lipid-A and several rough chemotypes of LPS from *E. coli* have determined the structural polymorphism of aggregates formed by these chemotypes in the presence of $MgCl_2$ at different levels of hydration and at different temperatures.[6,7]

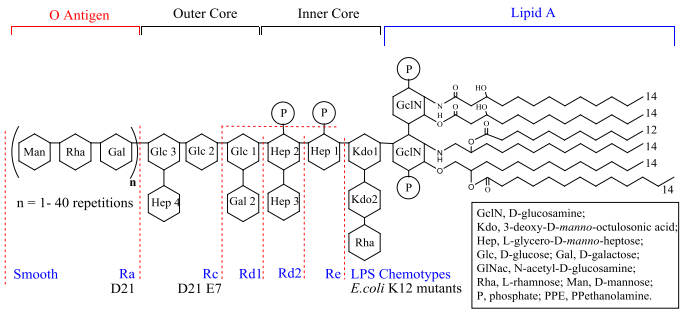

Figure 1: Possible structures of diverse smooth and rough (Ra to Re) LPS chemotypes expressed by *E. coli* bacterial strains. In the figure are reported the K12 mutants used in the experiments (D21 and D21E7).

These and more recent investigations[8,9] suggest that non-lamellar aggregate morphologies of LPS, such as cubic and inverted hexagonal phases,[7] exhibit greater toxicity than lamellar morphologies, a finding which has led the proposal of the conformational concept of endotoxicity.[8]

The idea that LPS toxicity is aggregate phase-dependent opens up new possibilities for the study and development of anti-endotoxic agents which interact with LPS aggregates and alter their morphologies. A useful starting point for investigating such putative anti-endotoxic substances is to examine the action of mammalian cationic antimicrobial peptides (AMPs), since in addition to their anti-infective activity,[10] some AMPs also bind to LPS and reduce its toxicity.[11–14] The majority of studies on LPS-peptide interactions have involved the shorter headgroup rough LPS chemotypes, without consideration of the more commonly expressed smooth chemotypes.[11,13,14] To date, most studies concerning the putative mechanism of AMPs in attenuating toxicity through altering LPS aggregate structure have been carried out at a non-physiological, high LPS concentration and with an excess of peptide;[11,13,14] as a consequence of this, the hypothesis of the morphology/toxicity relationship originating from these studies may present some limitations.

In this investigation we have used small-angle neutron scattering (SANS) and cryogenic transmission electron microscopy (cryoTEM) to examine the interaction of the human cathelicidin (LL37) and the bovine lactoferricin (LFb) with both smooth and roughs LPS chemotypes from *E. coli* 0111B4 and two K12 D21 mutants. Both the α-helical LL37 and the

β-sheet LFb amphiphatic peptides have shown interesting anti-inflammatory activity either *in vitro* or *ex vivo*.[11,15–17]

The comparison between the peptides LL37 and LFb may help to explain the mechanism of action of AMPs as anti-endotoxic agents and the apparent higher efficacy of the α-helical LL37 compared to the β-sheet LFb.[18]

To date only two studies[19,20] have used SANS to determine the structure of lipid-A and Re LPS colloidal aggregates in solution at concentrations more physiologically relevant than those used in earlier X-ray diffraction experiments. By combining the SANS measurements with the cryoTEM technique our aim has been to define the morphological changes induced by using mathematical models which are relevant to the complex morphologies observed in the samples.

Experimental section

Materials

Lysogeny broth (LB), Kimax boro-silicate centrifuge tubes, liquefied phenol $\geq$ 96% pure, deuterium oxide D_2O 99.990 atom % D and magnesium chloride anhydrous were all purchased from Sigma-Aldrich Ltd. (Dorset, UK). LPS 0111B4 was purchased from Merck KGaA (Darmstadt, Germany). Petroleum ether (40-60 degree) was obtained from VWR International (Soulsbury, UK). Chloroform and diethyl ether were obtained from Fisher Scientific (Loughborough, UK). All the solvents were of HPLC grade or higher. The human cathelicidin peptide LL37 was purchased from GenScript USA Inc. (Piscataway, USA) . The bovine lactoferricin peptide LFb used in these experiments is the fragment of the bovine lactoferrin protein from residue 17 to residue 41 and was purchased from Alpha Diagnostic International Inc. (Sant Antonio, USA). The ultrapure water used throughout was produced by a Purelab Ultra machine from ELGA process water (Marlow, UK), with a specific resistivity of 18.2 M$\Omega \cdot cm$.

Extraction of rough LPS from *E.coli*

The liquid phenol-chloroform-petroleum ether (PCP) extraction of Galanos *et al.*[21] is generally considered the extraction method best suited for rough chemotypes of LPS such as LPS D21 and D21E7 and was therefore used for their extraction from bacterial cultures. However contaminants remain present at the end of the PCP extraction, especially nucleic acids, which co-partition in the same phase as the LPS.[22] Therefore in order to achieve a higher degree of purity, a few additional steps adapted from the Darveau LPS extraction method[23] were added to the Galanos method. The additional steps included the enzymatic digestion of protein and nucleic acids followed by dialysis and ultracentrifugation of the extract obtained from the PCP extraction.[23] In brief, cultures of *E. coli* K12 mutants D21 and D21E7 were incubated for 10 hours at 37°C under constant agitation (170-200 rpm). The bacterial pellet was collected by centrifugation by the use of a Boeco U-320 bench centrifuge (Boeco, Hamburg, Germany) at 150 g for 20 minutes at 4°C and washed, followed by the PCP extraction methodology. The LPS extract resulting from this first step was suspended and enzymatically digested, followed by an ultracentrifugation step using a Beckman L8-M ultracentrifuge (Beckman Coulter Inc, Pasadena, USA) at 162000 g for 4.5 hours at 14°C as described by the Darveau extraction method. Subsequently a final PCP extraction was performed to remove any residual contaminants, then the final pure LPS extract was liophylized with a Heto Powerdry LL3000 freeze dryer (Thermo Scientific, Wilmington, USA) and stored at -20°C .

Sample preparation

The aggregates of LPS were prepared for cryoTEM and SANS experiments using the thin film hydration method. Briefly, a suspension of each LPS chemotype in organic solvent (chloroform:methanol 4:1 v/v) was transferred into a round-bottomed flask and the solvent was evaporated by means of a Buchi rotovapor system R-210 (Buchi Labortechnik AG,

Flawill, Switzerland) connected to a KNF Lab Neuberger Laboport Diaphragm Vacuum Pump UN840.3 FTP (KNF Neuberger UK, Witney, UK) and equipped with a Buchi water bath at 40°C until a film of LPS was formed. The film was re-suspended in D_2O containing 1 mM $MgCl_2$ as counter ions for the charges present in the LPS headgroups. The salt concentration was not chosen to mimic the host physiological ion concentration, but rather to reproduce the cross-linking effect of Mg^{2+} on LPS aggregates and on the surface of the bacterial membrane.[24,25] The experiments concerning the effect of the dilution on the SANS scattering pattern of LPS described below, were carried out using LPS concentrations of 4, 6, 8 and 10 mg/ml. For the interaction study with the peptides LL37 or LFb, an LPS concentration of 6 mg/ml was used and each peptide was added at the LPS/peptide ratios (w/w) of 50/1 and 10/1. The peptides were allowed to interact with the LPS for at least one hour prior to measurement.

Cryo transmission electron microscopy (cryoTEM)

The samples were processed and analysed by cryogenic transmission electron microscopy (cryoTEM) as follows. The cryoTEM investigations were performed using a Zeiss Libra 120 (Carl Zeiss NTS, Oberkochen, Germany). The microscope was operating at an accelerating voltage of 80 kV and in zero loss bright-field mode. Digital images were recorded under low dose conditions with a slow-scan CCD camera (TRS GmbH, Moorenweis, Germany) and iTEM software (Olympus Soft Imaging Solutions GmbH, Munster, Germany). An under-focus of 1-2 μm was used to enhance the image contrast. The cryoTEM specimen preparations were performed in a custom-built climate chamber at 25°C and approximately 98-100% relative humidity. A small drop ($\sim$1 μl) of sample was deposited on a copper grid covered with a carbon reinforced holey polymer film. Excess liquid was thereafter removed by means of blotting with a filter paper, leaving a thin film of the solution on the grid. Immediately after blotting the sample was vitrified in liquid ethane, held just above its freezing point of -182°C . Samples were kept below -165°C and protected against atmospheric conditions during both transfer to the TEM and examination, where representative images for

the samples were acquired. Full details of the technique are described in Almgren *et al.*[26] The rapid cooling rate prevents ice crystal formation and ensures that no structural rearrangements take place during the vitrification process. Thus, the cryoTEM images can be trusted to give an accurate picture of the structures existing in the bulk liquid samples. However, the limited thickness of the sample film ($\leq$0.5 μm) can lead to a potential exclusion of large particles and structures from the specimens. The cryoTEM analysis was repeated several times for each sample, and the images shown were chosen to give a representative picture of the structures observed while viewing a large number of different areas on the TEM grids.

Small-Angle Neutron Scattering (SANS)

The SANS measurements were carried out on the LoQ instrument at the ISIS pulsed neutron source at the Rutherford-Appleton Laboratory (Oxon, UK). This instrument produces an incident neutron beam with wavelengths of 2.2 - 10 Å in time of flight mode. The instrument has a broad range in scattering vector resulting in wide Q range of approximately 0.01 - 0.34 $Å^{-1}$; this can be achieved in one single measurement without the need to change the position of the detector. The beam is collimated into the sample after being framed at a defined beam size of 8 mm diameter. The 64 cm^2 active area of the detector is placed at 4.1 meters from the sample into a vacuum tube. A second detector placed at a closer position records the scattering at higher Q.[27]

The samples were placed in cleaned quartz cells of 1 mm path length and the scattering pattern was recorded at 37°C with an acquisition of at least 60 μA current (approximately one hour). The transmission and background scattering from the solution and solutes were subtracted from the samples prior to analysis. The data were analysed by means of mathematical models described in detail in the Supporting information section. Dilution experiments were carried out beforehand to exclude the structure factor contribution to the data fitting process. During the fitting process a constrained range of physically reasonable background scattering intensities were introduced into the calculations according to the experimental

and theoretical values for the buffer. The fits where accepted only if the deviation from the experimental data was within error.

Results

In this study the different chemotypes of lipopolysaccharide analyzed are the smooth LPS 0111B4 from *E. coli* 0111B4, the rough Ra LPS D21 from *E. coli* K12 mutant D21 and the rough Rc LPS E7 from *E. coli* K12 mutant D21E7 (Figure 1).

CryoTEM visualization of LPS aggregates and modifcations induced by the peptides

According to the cryoTEM micrographs, LPS 0111B4 at a concentration of 6 mg/ml in a 1 mM $MgCl_2$ solution forms elongated and branched worm-like micelles (Figure 2 A), in common with previous studies.[28] The micelles have an approximate diameter of 150 Å and wide mean inter-particle distances (estimated from the cryoTEM micrographs) probably due to charge repulsion and steric hindrance of the core oligosaccharide moieties and O-antigen; it must be considered however that the precise diameter value can not be calculated directly from the micrograph because of the low resolution of the image and the possibility that the micellles are flattened or twisted, as in the case of ribbon-like particles. The micelles have the tendency to form connected structures which could be described as toroids, depicted in Figure 3, which resemble loops of regular or irregular shape and different sizes.

The addition of LL37 peptide to LPS 0111B4 (Figure 2 B) prevented the formation of toroids and connections between the elongated micelles and the number of branched structures decreased in comparison to the LPS alone. The peptide appeared to halve the diameter of the chains to approximately 80 Å. LL37 also shortened the length of LPS 0111B4 micelles, augmented the number of smaller fragments and reduced the inter-particle space probably due to charge neutralization. The peptide LFb induced a smaller reduction of the diameter of the micelles to 115 Å. LFb had a lesser impact on the length of the particles than LL37

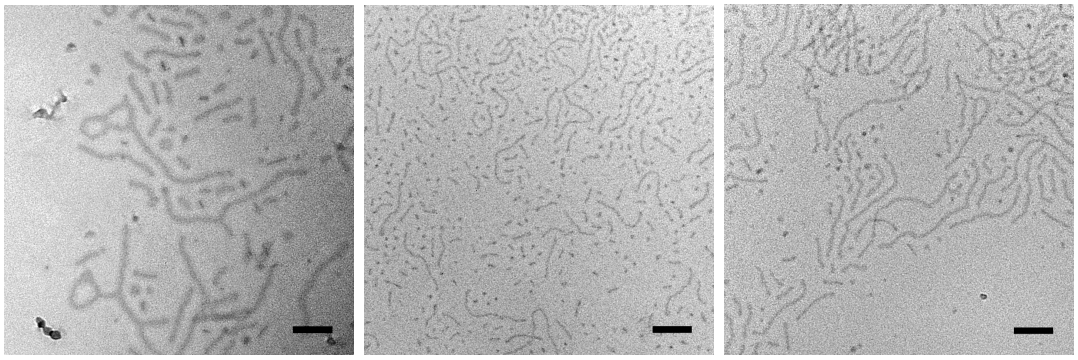

A B C

Figure 2: (A) CryoTEM micrographs of smooth LPS 0111B4 at 6 mg/ml in a 1 mM $MgCl_2$ solution forming elongated, branched micelles with some toroidal structures. Addition of (B) LL37 and (C) LFb peptides at the LPS/peptide ratio of 10/1: formation of thinner, shorter and less branched elongated structures. Size bar equal to 100 nm.

(Figure 2 C) and it seemed to cause a closer packing of the aggregates, with a visible reduction of the inter-particle spaces for the same reason described above. Frequently the micelles appeared connected and branched even in the presence of LFb peptide and toroidal structures or loops are scarcely present. LFb peptide similarly to LL37 also increased the number of smaller structures or fragments, probably due to a surfactant-like activity of the peptides in disrupting the micelles, which has already been observed for different AMPs.[28]

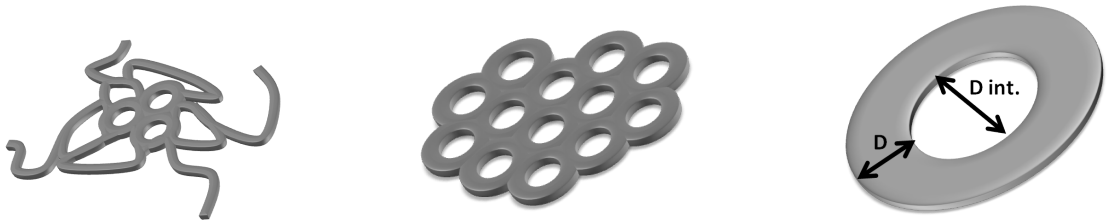

A B C

Figure 3: Diverse type of aggregate morphologies: (A) irregular micellar network and (B) regular toroidal structures. (C) Dimension of the toroid with the toroidal internal diameter *D Int.* and the diameter of the micelle *D*.

The LPS D21 at a concentration of 6 mg/ml in a 1 mM $MgCl_2$ solution forms mainly sheet-like structures distributed as single lamellae, possibly coexisting with toroids as outlined

in Figure 4 A. The resolution of the micrographs does not allow a more precise definition of such a structure, which in this case could be mistaken for ripples or undulations of the lamellae. In the micrograph the presence of small white holes, or dots, in the sheets is due to the effect of radiation damage on the sample; they can be easily distinguished from toroids and pores because of their white clear background.

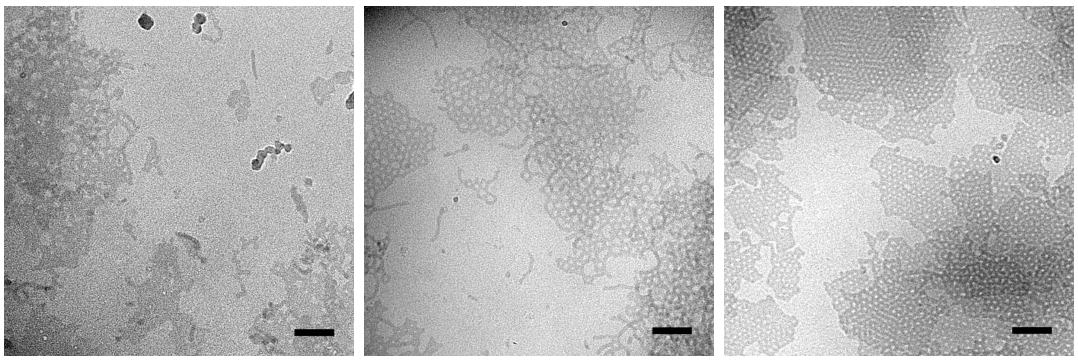

A B C

Figure 4: (A) CryoTEM of LPS D21 at 6 mg/ml forming sheet-like structures coexisting with toroids in a 1 mM $MgCl_2$ solution. (B) Addition of LL37 at LPS/peptide ratio of 10:1: formation of elongated particles closing up into irregular toroids. (C) Addition of LFb at LPS/peptide ratio of 10:1: regular toroids. Size bar equal to 100 nm.

LL37 induced the formation of a mixture of organized toroids and a network of elongated micelles (Figure 3 A and B) opening up into elongated micelles, as depicted in the micrograph of Figure 4 B. The micelles forming the toroids had a diameter (D) of ∼77 Å, however it was not possible to measure the inner diameter of the toroids because of the wide range of sizes and shapes. Toroidal structures were the most commonly visible structures with patches of uneven shapes and others with a more regular and ordered structure; some micelles were visible free from the network and formed elongated structures. The situation in the presence of LFb (Figure 4 C) showed a much more regular structure than in the presence of LL37, as described in Figure 3 B. The toroids formed appeared much more uniform in terms of shape and dimensions, with an homogeneous toroidal pattern; the micelles forming the toroids had a diameter of approximately 82 Å and the toroidal internal diameter was approximately 78 Å; this structure resembles lamellae which have been perforated by regularly-spaced pores

(Figure 4 C).

The LPS E7 at a concentration of 6 mg/ml in a 1 mM $MgCl_2$ solution forms irregular sheets with an undulating surface (Figure 5 A) in which some holes are present. The addition of LL37 caused the formation of mixed sheet-like structures together with irregular toroids (Figure 3 A) and elongated micelles, the latter having an approximate diameter of 90 Å (Figure 5 B).

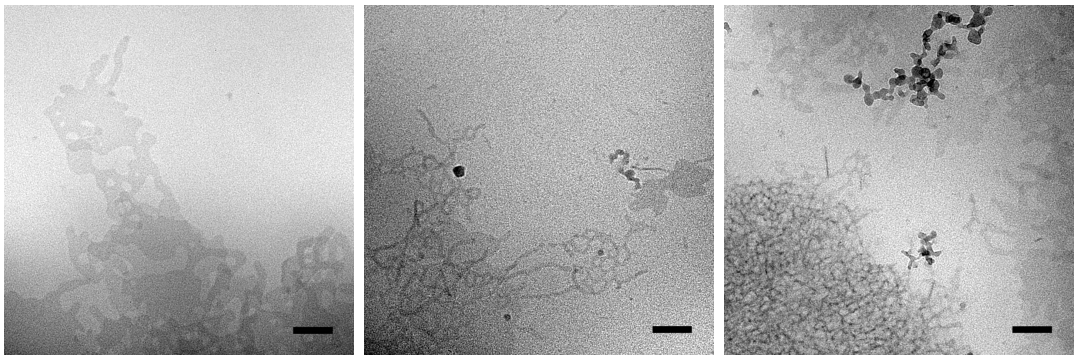

A B C

Figure 5: (A) CryoTEM of LPS E7 at 6 mg/ml in a 1 mM $MgCl_2$ solution forming undulated, irregular lamellae. (B) addition of LL37 at LPS/peptide ratio of 10:1: formation of elongated particles closing into toroids and lamellae. (C) Addition of LFb at LPS/peptide ratio of 10:1: formation of mixed thin elongated particles and lamellae. Size bar equal to 100 nm.

LFb peptide added to LPS E7 induced the formation of mixed irregular sheets and very thin elongated structures for which the inter-particle space was not clearly distinguishable and it was not possible to measure the diameter of these chains from the micrographs (Figure 5 C). The micrographs showed a few patches of possible toroidal structures.

SANS investigation of LPS aggregates and modifications induced by the peptides

The Kratky-Porod approximation[29,30] (details in Supporting information) is useful for analyzing data from particles which are more flexible than simple rods. Hence the data for the LPS 0111B4 dilution study was plotted as $ln[Q \times (\delta\Sigma/\delta\Omega)(Q)]\, vs\, Q^2$ in Figure 1 (Supporting information). The linear fitting of the data in the intermediate-high Q range 0.032-0.067

(equivalent to a Q^2 range of 0.00102-0.00449) allowed the calculations of the parameters reported in Table 1 (Supporting information), as described by Equations 5 and 6 (Supporting information). Additionally the plot allows the calculation of the mass per unit length M_L in Da/Å according to Equation 7; in this calculation the parameters considered are the particles scattering length density (SLD) ρ_{worm} of 1.57×10^{10} cm^{-2}, the solvent SLD $\rho_{solvent}$ of 6.35×10^{10} cm^{-2} and a density of LPS equal to 1.4 g/cm^3 as reported by Ulevitch[31] .

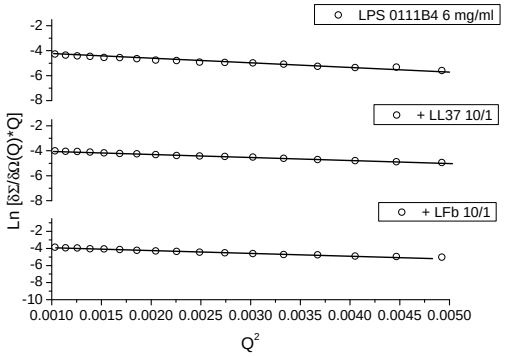

Figure 6: Kratky plot of LPS 0111B4 (6 mg/ml) in 1 mM $MgCl_2$ solution at 37°C alone and with the addition of peptides LL37 or LFb at a LPS/peptide ratio of 10/1. The linear fit was applied at the intermediate-high Q^2 range of 0.001-0.005.

Table 1: Values from the linear fitting of Kratky plot of LPS 0111B4 (6 mg/ml) in 1 mM $MgCl_2$ solution at 37°C alone and following challenge by the peptides LL37 or LFb at the intermediate-high Q^2 range of 0.001-0.005.

Sample	R^2 fit	R_g (Å)	$R = \sqrt{2} \times R_g$ (Å)	M_L (Da/Å)
0111B4 6 mg/ml	0.973	25.2±0.7	36	108855±992
+ LL37 50/1	0.974	24.9±0.7	35	104677±943
+ LL37 10/1	0.995	22.5±0.3	32	101600±326
+ LFb 50/1	0.979	25.4±0.6	36	102703±881
+ LFb 10/1	0.985	25.4±0.5	36	96710±739

The Kratky analysis applied to these dilutions experiments estimate that the radius of the worm-like micelle did not change significantly and maintained values between 35 and 37 Å at all the dilutions tested. Being inversely proportional to the concentration of the solute, M_L increases with decreasing concentration and can be used to estimate the amount

of molecules present over the size of the micelle. Unfortunately being a structurally polydisperse molecule, this makes it difficult to calculate this number, but according to Aurell *et al.* the average molecular weight of LPS 0111B4 was estimated to be 10000 Da[32] . Therefore we can see how the number of molecules per micelle increases as the concentration decreases. The Kratky-Porod model was applied to the data from the experiments containing the peptides. In Figure 6 only the fitting for the 10/1 LPS/peptide ratio is depicted as an example. The linear fit at the intermediate-high Q range gave the values for the parameters listed in Table 1. A significant reduction in R_g was not observed except for the sample containing the highest concentration of LL37 peptide (ratio 10/1). No modification of M_L was observed in the presence of the two peptides. All LPS D21 dilutions were fitted as a monodisperse oriented sheet with a shell/core/shell feature[33] (Figure 6) using the SANS data fitting software FISH,[34] for which the equations are described in the Supporting information. In this case the shell was considered as being formed by the hydrophilic regions of LPS (the oligosaccharide group), and the core being composed of the hydrophobic acyl chains of the lipid-A region. The fitting of the data reported in Figure 2 shows the scattering curves of D21 at different concentrations. At 4 mg/ml and 6 mg/ml the mono-disperse oriented sheet fitting is acceptable, while at higher concentrations (8 mg/ml and 10 mg/ml) the sheet features are lost and the model gives a less precise fit (see SSE values reported in Table 2 in Supporting information). It is interesting to note the formation of three shoulders at high concentrations which are not visible in the scattering curve at 4 mg/ml; these might be Bragg reflections from a multi-lamellar or non-lamellar aggregate structure.[6,7] If these reflections are grouped in equidistant ratios of the lamellar repeat *d-spacing* we can approximate the value of the distance repeat as $d = \frac{2\Pi}{Q}$; the resulting *d-spacing* values between bilayers calculated at high Q range (Q value of the first reflection on the right) for D21 at 6 mg/ml, 8 mg/ml and 10 mg/ml are respectively 71 Å, 58 Å and 60 Å; the ripples at lower Q values are separated from the first reflection by a ratio of respectively 0.41 ± 0.05, 0.40 ± 0.09 and 0.41 ± 0.09 which suggests a repeated distance between $1/\sqrt{6}$ and $1/\sqrt{7}$; such value of repeated distance at higher LPS concentration may suggest the presence of non-lamellar features (cubic or

inverted hexagonal phase) as previously described for rough LPS at high concentration by Seydel *et al.*[7] The absence of non-lamellar features at the lowest LPS concentration highlight how the concentration plays a crucial role on the morphology of LPS aggregates, emphasizing the need of biophysical studies at the lowest LPS concentration possible as a mimic for physiological conditions. However, the formation of ripples might also suggest the formation of different populations of objects which could be either sheets with different thickness or alternatively particles with diverse morphologies. This might explain the conserved nature of the middle reflection (Q 0.032) which would describe one population that does not change with the dilutions, together with other populations described by the other peaks at diverse Q values. Due to the complexity of the system, an adequate model to fit this data fully is not available, although several attempts to mix different form factors were made unsuccessfully. The output parameters of the monodisperse oriented sheet shell/core/shell model provided by the FISH software are reported in the Table 2 in Supporting information. The contrast value was fixed in the model and was calculated to be 0.904 for LPS D21, according to Equation 10. The values of the bilayer's shell and core thickness did not change with the increasing concentration of LPS, therefore the thickness T is similar at all the dilutions (between 55 and 58 Å). The scale factor decreased because it is proportional to the power of $R\sigma$.

The SANS data of the samples containing LPS D21 at the concentration of 6 mg/ml in the presence of the peptides, either LL37 or LFb, were initially analyzed with the Kratky and the Guinier approximations respectively (data not shown), in order to narrow down the possible usable form factors. Subsequently, the LPS D21/LL37 and LPS D21/LFb samples were fitted to respectively a Kholodenko flexible cylinder model[35] and a monodisperse sheet shell/core/shell model[33] with the use of FISH software. LPS D21/LL37 fitting is shown in Figure 7 (red line) and the resultant parameters are reported in Table 2. The value of the contrast is 8.17e-01 (see Equation 10 in Supporting information). According to fits for the Kholodenko flexible cylinder model, the number of segments n appeared to reduce upon addition of more LL37, whilst the Khun length (l) seemed scarcely affected. Overall the

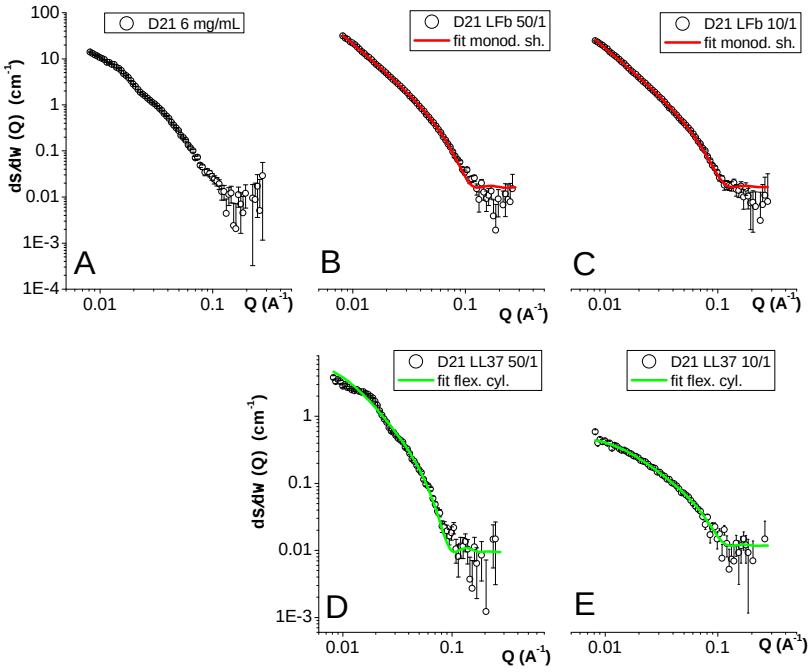

Figure 7: Scattering pattern of LPS D21 6 mg/ml concentration in a 1 mM $MgCl_2$ solution at 37°C (A). Addition of the peptides, either LL37 (B and C) or LFb (D and E), at LPS/peptide ratios of 50/1 and 10/1. B and C) LPS D21 with LFb fitted with the monodisperse sheet shell/core/shell model (red line). D and E) LPS D21 with LL37 fitted with the Kholodenko flexible cylinder model (green line).

total length of one single particle reduced at higher concentration of LL37. The core radius (r_c) decreased from the peptide ratio 50/1 to 10/1, whilst the shell thickness (t_s) was not influenced by the increased concentration of peptide. The contrast value was constant and introduced into the fitting as explained above. The volume fraction (ϕ) for each sample was also calculated from the $Scale factor$ value, and they did not match the calculated theoretical value for LPS D21 alone which is 0.004267 (see Supporting Information); this is consistent with the presence of the peptide within the micelle which is likely to alter the density and the SLD of the aggregates.

The scattering curves of LPS D21/LFb peptide were fitted with the lamellar model described previously, as if the lamellae of LPS D21 was perforated by LFb in regular toroids or pores. As with the LPS D21/LL37 sample, the contrast value input into the model was fixed; the model provides a close fit to the scattering curves (Figure 7) and the resulting values for the parameters are presented in Table 2. At the LPS/peptide ratio of 50/1, core thickness

Table 2: Kholodenko flexible cylinder model parameters of the fitting of LPS D21 at 6 mg/ml in a 1 mM $MgCl_2$ solution at 37°C with the peptide LL37 at LPS/peptide ratios of 50/1 and 10/1.

D21 6 mg/ml	+ LL37 50/1	+ LL37 10/1
Scale factor	4.58 e-07	2.18 e-07
ϕ [a]	1.39 e-04	6.60 e-05
n	13 ±7	8 ±2
l (Å)	109 ±36	103 ±17
total L (Å)	1397	816
r_c core (Å)	21 ±1	13 ±1
t_s shell (Å)	17 ±3	17 ±1
total R (Å)	38	30
SSE [b]	1.08 e+03	6.64 e+01

[a] calculated volume fraction from the *Scale factor* according to Equation 9; [b] sum of squared errors.

(t_c) and shell thickness (t_s) values did not change considerably compared to the LPS D21 alone, with a reduction of both t_c and t_s of approximately 1-1.5 Å each; increasing the concentration of the peptide to a LPS/peptide ratio of 10/1, the core thickness increased while the shell layer became thinner. In this case the overall T of the bilayer reduced by ∼10% compared to the bilayer without the presence of LFb. The volume fraction ϕ values increased with the addition of the peptide at both the LPS/peptide ratios.

The fitting of LPS E7 dilutions (Figure 3, Supporting information) as monodisperse sheet shell/core/shell was appropriate in consideration of the data obtained from the cryoTEM experiment, and the output parameters (Table 3, Supporting information) confirm that the concentration did not change the lamellar thickness. In detail both the shell and the core thickness, t_s and t_c respectively, are similar for each dilution and the value of $R\sigma$ does not change significantly except for the LPS E7 sample 8 mg/ml in which it increased. The scattering curve of LPS E7 retained the same shape for each concentration and the scattering intensity increased, as expected, with the increase in LPS concentration.

Since it is likely that the samples containing rough Rd LPS E7 at 6 mg/ml concentration in solution containing 1 mM $MgCl_2$, at 37°C , with the addition of the peptides LL37 or LFb at LPS/peptide ratios of 50/1 and 10/1, consisted of a mixture of structures, both a lamellar

structure model and a flexible cylinder structure model were applied to the SANS data. The application of the monodisperse shell/core/shell model is shown in Figure 8 (red lines) for LL37 and LFb peptides. The model fitted closely the scattering curves and produced the parameters reported in Table 3. The peptide LL37 reduced the overall thickness of the lamellae with the increase in the peptide concentration. This effect was mostly concentrated on the shell part of the bilayer, as a matter of fact the thickness of the hydrophobic core is almost unchanged at the highest concentration of peptide (ratio LPS E7/LL37 of 10/1). The value of $R\sigma$ was halved exclusively at the highest concentration of peptide, compared to the value of LPS E7 alone, suggesting an increase in the order of the system. The volume fraction remained fairly constant for all the three samples within the LL37 group. The addition of LFb peptide had a more variable effect on the bilayer (see parameters in Table 3). Compared to the sample without peptide, the data for LPS E7/LFb ratio of 50/1 presents a small total thickness reduction coupled with a larger increase of the core thickness t_c at the expense of a decrease of the shell thickness t_s. At the highest concentration of LFb (ratio 10/1) there is a drop of total thickness of $\sim$3 Å mainly due to a reduction of the core thickness t_c, this effect contrasts with the effect noted at lower LFb concentration at the LPS/peptide ratio of 50/1. The value of $R\sigma$ has showed a slight reduction upon addition of the peptide LFb suggesting a limited increase in the system's order, and it was constant for both peptide ratios. LFb seems to induce a low reduction of the volume fraction, compared to the less pronounced effect on the volume fraction ϕ of the peptide LL37.

The LPS E7 alone forms lamellar structures, therefore a direct comparison with the samples containing the two peptides fitted using the Kholodenko model (Figure 8, green lines) is not possible. From the parameters obtained from the fitting reported in Table 3 it is possible to observe that the scale factors and the volume fractions for all the samples remain unchanged. Considering the effect of both LL37 and LFb it is striking to note the value of number of segments (n) and length of each segment (l), where both peptides induced the formation of a large number (ranging form 4000 to 48000) of very short segments of micelles of approximately 8 to 11 Å. In the case of LL37 peptide, the highest peptide concentration

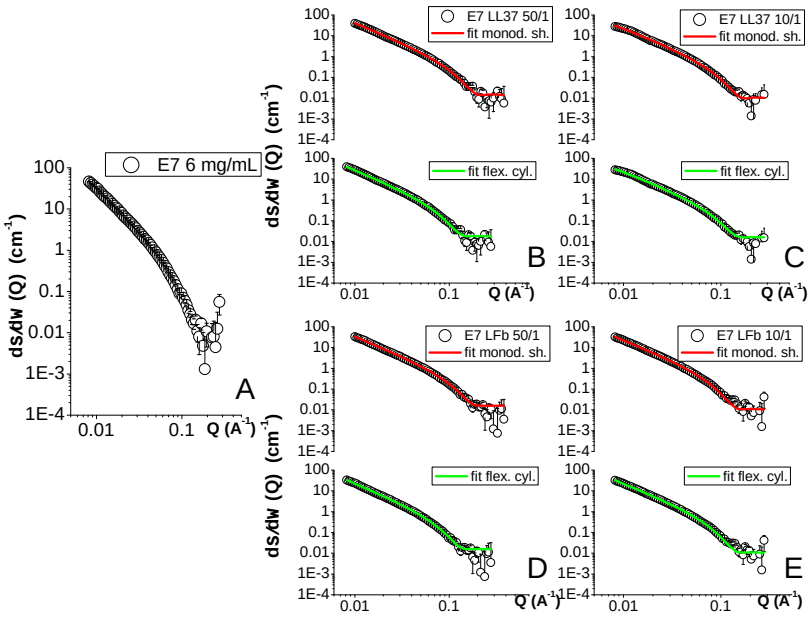

Figure 8: A) Scattering pattern of the LPS E7 (6 mg/ml) in solution containing 1 mM $MgCl_2$ at 37°C and with the peptides,either LL37 (B and C) or LFb (D and E), at LPS/peptide ratios of 50/1 and 10/1. Fittngs of the scattering curves with the monodisperse sheet shell/core/shell model (red line) and the Kholodenko flexible cylinder model (green line).

(ratio 10/1) revealed a ten-fold reduction of n compared to the 50/1 ratio, while the l value is increased from 8 to 10 Å. However the large errors must be considered. The core radius and the shell thickness did not undergo major changes apart from a reduction of radius of the core (r_c) from 9 to 8 Å and the total radius of the objects is set between 23-24 Å. The peptide LFb induced a six-fold reduction of n and a l increase from 9 to 11 Å , moreover the peptide induced a considerable reduction of the core from 11 to 8 Å and a less consistent reduction of the shell thickness of the cylinder.

Discussion

Due to the high polidispersity of the LPS structures formed, the cryoTEM experiments were specifically designed to guide the interpretation of the SANS data, allowing the application of models with greater relevance to the observed aggregate morphologies. Previous studies

Table 3: Parameters obtained from the monodisperse sheet shell/core/shell and the Kholodenko flexible cylinder model fittings of LPS E7 at 6 mg/ml in a 1 mM $MgCl_2$ solution at 37°C alone and with the peptides LL37 or LFb at LPS/peptide ratios of 50/1 and 10/1.

	E7 6 mg/ml	+LL37 50/1	+LL37 10/1	+LFb 50/1	+LFb 10/1
	Monodisperse sheet shell/core/shell model				
Scale factor	0.623	0.527	0.136	0.365	0.406
ϕ [a]	0.00468	0.00415	0.00432	0.00408	0.00338
t_c (Å) [b]	17±0	16±0	17±2	21±1	16±0
t_s (Å) [c]	13±0	13±0	11±1	10±1	13±0
T (Å) [d]	43	42	39	41	39
$R\sigma$ (Å)	770	734	372	702	695
SSE [e]	1.39 e+02	2.07 e+02	6.25 e+02	1.11 e+02	7.72 e+01
	Kholodenko flexible cylinder model				
Scale factor		2.02 e-07	2.18 e-07	2.19 e-07	2.09 e-07
ϕ [f]		6.11 e-05	6.59 e-05	6.62 e-05	6.33 e-05
n		48698 ±25330	4877 ±1687	61979 ±8877	13788 ±3653
l (Å)		8±1	10±2	9±0	11±0
total L (Å)		407915	48948	524625	155352
r_c (Å)		9±0	8±1	11±0	8±0
t_s (Å)		16±0	15±1	14±0	16±0
total R (Å)		25	23	25	24
SSE [e]		1.90 e+02	5.65 e+02	1.19 e+02	1.46 e+02

[a] calculated volume fraction from the *Scale* according to Equation 14; [b] core thickness; [c] shell thickness; [d] Total thickness $T = 2 \times t_s + t_c$; [e] sum of squared errors; [f] calculated volume fraction from the *Scale* according to Equation 9.

using dynamic light scattering focused only on the determination of the aggregate size distribution of one LPS chemotype upon addition of AMPs[36] to make assumptions about role of the putative morphology-activity dependency of toxicity.[11–13] The diversity of aggregate morphology (Figure 3) is dependent upon the solution conditions and the physico-chemical characteristics of both the LPS chemotypes and the peptides. The changes induced by LL37 and LFb to the LPS aggregates (Figure 4 in Supporting Information) appeared dependent upon the peptide conformation, charge and hydrophobicity. Despite a lower net positive charge of LL37 (+6) compared to LFb (+8), the greater effects shown by LL37 may be related to its amphiphilic α-helix which facilitates the interaction with membranes and aggregates containing LPS via an efficient balance between electrostatic and hydrophobic

forces,[18] resulting in the displacement of stabilizing Mg^{+2} ions.[24]

Previous freeze-fracture TEM (ffTEM) and cryoTEM analysis of the *E. coli* 055B5 smooth LPS in PBS reported the formation of spherical aggregates[37,38] but did not consider the effects of divalent cations on the morphologies of LPS aggregates.[39] Here the aggregation of smooth LPS 0111B4 was investigated in the presence of 1 mM $MgCl_2$, as divalent cations naturally cross-link and stabilise LPS in outer membrane,[25] facilitating the formation of worm-like micelles observed by cryoTEM and modelled from the Kratky approximation of the SANS data.

The electrostatic attraction between the AMPs and negatively charged lipid or LPS head-groups (*i.e.* core oligosaccharide and lipid-A phosphates in LPS) is the dominant driving force of the interaction.[24,40] The tendency of many cationic peptides (especially α-helical ones) to bind to lipidic structures with high positive curvature and induce further curvature, is well established,[41] and this may also be the case for the elongated LPS 0111B4 micelles. The cryoTEM micrographs of LPS 0111B4 with LL37 and LFb, showed short unbranched elongated micelles which clearly present higher mean curvature than the longer, branched micelles present without peptides. The observed reduction in micelle thickness and smaller inter-particle distance may be due to the presence of peptides in the core oligosaccharide region, leading to charge neutralization and reduction in the electrostatic repulsion between micelles, and shortening of the oligosaccharide chains. Despite the changes seen in the micrographs, the SANS data suggest a minimal effect of both peptides on LPS 0111B4 (Figure 4, Supporting information). The SANS technique is more sensitive to changes in the micellar hydrophobic region therefore the lack of scattering pattern modification upon addition of the peptides suggests neither LL37 nor LFb penetrate into the hydrophobic lipid-A region but may bind to the phosphates of the core oligosaccharide. The cryoTEM of D21 Ra LPS show the formation of complex lamellar structures similar to those seen by TEM performed on the same D21 Ra chemotype.[42] More recently Richter *et al.*[43] found that Ra LPS from *S. minnesota* R60, analyzed by freeze-fracture TEM (ffTEM) and cryoTEM, forms elongated fibrils made up of two tightly packed bilayers in 20 mM HEPES buffer. The apparent dis-

crepancy between the data reported in the current study and those reported by Richter *et al.* can be explained by the tendency of Mg^{2+} to induce an increase in the lamellarity of the aggregates.[7]

SANS data fitting for the different dilutions of LPS D21 confirmed the presence of lamellar structures (Figure 4), the thicknesses of which were not affected by concentration. The formation of fringes in the scattering curve at higher concentrations, suggests that the system becomes more ordered and rigid and potentially forming non-lamellar structures.

The addition of LL37 to the LPS D21 caused an increase of the positive curvature and the subsequent formation of elongated particles, closing up into a micellar network as shown by cryoTEM micrographs (Figure 4). In this regard, SANS data showed a decrease of the number of LPS molecules per unit length of the micelles upon addition of LL37, suggesting that the peptide acts on the inner core oligosaccharide of the LPS D21, and possibly on the lipid-A region as well, affecting its packing by inserting into the micelle and reducing the density of LPS molecules. LPS D21 mixed with LFb forms tightly packed, regular toroids which resemble a perforated lamellae (Figure 4, Supporting information). Such a complex system could not be analyzed as a flexible micelle model therefore it was approximated as a bilayer. The monodisperse shell/core/shell model shows most of the thickness changes induced by LFb occur in the bilayer shell and thus may not partition into the bilayer but remains at the solvent/lipid interface.[44] It has been proposed that LFb has no bacterial membrane penetrating properties but acts on the surface of the membrane depolarizing it and causing positive curvature.[45] The regular D21/LFb structures observed by cryoTEM could result from the localised curvature induced by the peptide on the LPS lamellae.

The exposure of the core oligosaccharide and the lipid-A phosphate groups of LPS D21, allows for the stronger interaction of both peptides with the hydrophobic core of the aggregates, compared to smooth LPS. LL37 influences the hydrophobic core of the LPS (the lipid-A acyl chains), to a greater extent than LFb, possible due to its facially amphiphilic α-helix which facilitates deeper membrane penetration.[46,47]

The cryoTEM micrographs for E7 Rc LPS show complex lamellar structures with some

micellar networks (Figure 4, Supporting information). Previous cryoTEM studies on *S. minnesota* Rc LPS in HEPES buffer reported the formation of elongated particles[48] and ffTEM investigations of the same system show mixtures of spherical liposomes and planar bilayers.[43] The latter findings and the data presented in this study are supported by X-ray diffraction of *S. minnesota* Rc LPS with Mg^{2+}.[7] According to the fits for the SANS data, dilution of the E7 LPS has no effect on the lamellar structures formed. The high $R\sigma$ values indicate a system without a rigid geometry, probably due to a heterogeneous population of highly undulating lamellae, prevented from any long-range association, hence the absence of fringes in the scattering curves.

With LL37, LPS E7 forms a mixed population of lamellae, micellar networks and worm-like micelles (Figure 4, Supporting information). The SANS data set for LPS E7/LL37 samples were analyzed as lamellar structures revealing that LL37 partially affects the shell thickness rather than the core of the aggregates. Whereas, when analysed as flexible cylinders, most of the modifications on the micelles occurred at the hydrophobic core level, reporting a radius of the micelle almost half that of the lamellar hydrophobic core thickness but, by contrast, no detectable changes in the number of molecules per unit length was observed, suggesting no modification to the lipid-A region of LPS. Despite the heterogeneous population of structures observed at the higher LL37 concentration, the value of $R\sigma$ suggests an unexpected increase of the order of the system, confirmed by the appearance of fringes in the scattering curve, which is difficult to explain from the data obtained. The cryoTEM showed that the addition of LFb to LPS E7 caused similar morphological changes to those of LL37 (Figure 4, Supporting information). As with the LPS D21 case, the SANS data were analyzed both as lamellae and elongated particles. LFb induced a general decrease in the lamellar thickness but interestingly the lowest LFb concentration (LPS/peptide ratio of 50/1) has a bigger impact than the 10/1 ratio when the values of t_c and t_s are compared. This might be due to a limitation of the model when it comes to the analysis of such a complex system. The analysis of LPS E7 challenged by the LFb as elongated objects revealed that increasing concentrations of peptide do not affect the radius and the mass per unit length of the particles.

Both LL37 and LFb peptides interact with the aggregates of LPS E7 to such an extent that the system became extremely complex and the intricacy of the data interpretation reflects such complexity. The heterogeneity of the aggregates did not allow for a precise analysis of the SANS data. What is clear is that the removal of the shielding of part of the core of LPS and the phosphates at the heptose level allows for a more intimate interaction of the peptides with the LPS E7 lipid-A phosphate groups inducing a higher positive curvature on the aggregates. The higher number of LPS E7 molecules in the samples, compared to the experiments carried out with LPS 0111B4 and D21, may result in an uneven distribution of the peptide where different regional concentrations accounts for the lack of uniformity of the samples, giving rise to the different morphologies observed.

Conclusion

Neither LL37 nor LFb are able to greatly modify the elongated micelles of LPS 0111B4, most likely due to a pre-existing high positive curvature of the aggregates, associated with the presence of the intact O-antigen so the interaction of both peptides with the elongated micelles induced limited modification on the micellar radii and length. Without the O-antigen, LPS D21 and E7 formed lamellar structures with a lower positive curvature which were more noticeably affected by the propensity of cationic peptides to induce positive curvature. LL37 in particular, is more effective than LFb in the modification of the core of the aggregates most likely due to its propitious physico-chemical properties (*i.e.* amphiphilicity, helical conformation, hydrophobicity, polar angle and charge[46]). The further removal of some of the core LPS as in the case of LPS E7, allowed for the direct interaction of the peptides with the innermost lipid-A region allowing both the peptides to induce high positive curvature, with the formation of heterogeneous aggregate morphologies most likely due to localized differences in peptide concentration. The conformational concept of endotoxicity states that some antimicrobial peptides may be able to reduce the toxicity of LPS by the lamellarization of the aggregates (*i.e.* reducing positive curvature). From our investigation

we show that both LL37 and LFb have the tendency to increase the positive curvature of both smooth and rough LPS chemotypes. Although it was previously observed that peptides derived from human LF fragments[11,49] reduce LPS toxicity inducing the lamellarization of the aggregates, our investigation revealed that this is not the case for intact LFb calling into question the role of LPS aggregate morphology in toxicity. The combination of SANS and cryoTEM techniques proved to aid our understanding of the activity of antimicrobial peptides interacting with LPS aggregates at biologically relevant concentrations, although further investigations using these techniques together with other biophysical tools (NMR, IR, fluorescence) are needed in order to develop advanced and sophisticated structural models.

Acknowledgement

This research was financially supported by a Next Generation Facility Users Grant (EPG0685691) from the UK Engineering and Physical Sciences Research Council. The authors thank Professor Rob Evans (Brunel University, UK) for the generous gift of the peptide bovine Lactoferricin (LFb) used in these experiments.

Supporting Information Available

Supporting Information are provided which include additional data obtained from the data fitting process, a schematic representation of the morphological modifications of LPS aggregates upon addition of the AMPs, the description of the fitting procedure used in the scattering data analysis. This information is available free of charge vie the Internet at http://pubs.acs.org/.

References

(1) Loppnow, H.; Brade, H.; Dürrbaum, I.; Dinarello, C. A.; Kusumoto, S.; Rietschel, E. T.; Flad, H. D. IL-1 induction-capacity of defined lipopolysaccharide partial structures. *J. Immunol.* **1989**, *142*, 3229–3238.

(2) Cohen, J. The immunopathogenesis of sepsis. *Nature* **2002**, *420*, 885–891.

(3) Raetz, C. R. H.; Whitfield, C. Lipopolysaccharide Endotoxins. *Ann. Rev. Biochem.* **2002**, *71*, 635–700.

(4) Rietschel, E. T.; Galanos, C.; Tanaka, A.; Ruschmann, E.; Luderitz, O.; Westphal, O. Biological Activities of Chemically Modified Endotoxins. *Eur. J. Biochem.* **1971**, *22*, 218–224.

(5) Gutsmann, T.; Schromm, A. B.; Brandenburg, K. The physicochemistry of endotoxins in relation to bioactivity. *Int. J. Med. Microbiol.* **2007**, *297*, 341–352.

(6) Brandenburg, K.; Koch, M. H.; Seydel, U. Phase diagram of deep rough mutant lipopolysaccharide from Salmonella minnesota R595. *J. Struct. Biol.* **1992**, *108*, 93–106.

(7) Seydel, U.; Koch, M. H.; Brandenburg, K. Structural Polymorphisms of Rough Mutant Lipopolysaccharides Rd to Ra from Salmonella minnesota. *J. Struct. Biol.* **1993**, *110*, 232–243.

(8) Brandenburg, K.; Andrä, J.; Müller, M.; Koch, M. H.; Garidel, P. Physicochemical properties of bacterial glycopolymers in relation to bioactivity. *Carbohydr. Res.* **2003**, *338*, 2477–2489.

(9) Brandenburg, K.; Hawkins, L.; Garidel, P.; Andrä, J.; Müller, M.; Heine, H.; Koch, M. H. J.; Seydel, U. Structural Polymorphism and Endotoxic Activity of Synthetic Phospholipid-like Amphiphiles. *Biochemistry* **2004**, *43*, 4039–4046.

(10) Zasloff, M. Antimicrobial peptides of multicellular organisms. *Nature* **2002**, *415*, 389–395.

(11) Andrä, J.; Lohner, K.; Blondelle, S. E.; Jerala, R.; Moriyon, I.; Koch, M. H. J.; Garidel, P.; Brandenburg, K. Enhancement of endotoxin neutralization by coupling of a C12-alkyl chain to a lactoferricin-derived peptide. *Biochem. J.* **2005**, *385*, 135–143.

(12) Hammer, M. U.; Brauser, A.; Olak, C.; Brezesinski, G.; Goldmann, T.; Gutsmann, T.; Andra, J. Lipopolysaccharide interaction is decisive for the activity of the antimicrobial peptide NK-2 against Escherichia coli and Proteus mirabilis. *Biochem. J.* **2010**, *427*, 477–488.

(13) Brandenburg, K.; Garidel, P.; Fukuoka, S.; Howe, J.; Koch, M. H. J.; Gutsmann, T.; Andrä, J. Molecular basis for endotoxin neutralization by amphipathic peptides derived from the alpha-helical cationic core-region of NK-lysin. *Biophys. Chem.* **2010**, *150*, 80–87.

(14) Kaconis, Y.; Kowalski, I.; Howe, J.; Brauser, A.; Richter, W.; Razquin-Olazarán, I.; Iñigo Pestaña, M.; Garidel, P.; Rössle, M.; Martinez de Tejada, G.; Gutsmann, T.; Brandenburg, K. Biophysical Mechanisms of Endotoxin Neutralization by Cationic Amphiphilic Peptides. *Biophys. J.* **2011**, *100*, 2652–2661.

(15) Burton, M. F.; Steel, P. G. The chemistry and biology of LL-37. *Nat. Prod. Rep.* **2009**, *26*, 1572–1584.

(16) Scott, A.; Weldon, S.; Buchanan, P. J.; Schock, B.; Ernst, R. K.; McAuley, D. F.; Tunney, M. M.; Irwin, C. R.; Elborn, J. S.; Taggart, C. C. Evaluation of the Ability of LL-37 to Neutralise LPS in Vitro and Ex Vivo. *PLoS One* **2011**, *6*, 26525.

(17) Kim, J. S.; Ellman, M. B.; Yan, D.; An, H. S.; Kc, R.; Li, X.; Chen, D.; Xiao, G.; Cs-Szabo, G.; Hoskin, D. W.; Buechter, D. D.; Van Wijnen, A. J.; Im, H.-J. Lactoferricin mediates anti-inflammatory and anti-catabolic effects via inhibition of IL-1 and LPS activity in the intervertebral disc. *J. Cell. Physiol.* **2013**, *228*, 1884–1896.

(18) Yeaman, M. R.; Yount, N. Y. Mechanisms of antimicrobial peptide action and resistance. *Pharmacol. Rev.* **2003**, *55*, 27–55.

(19) Hayter, J. B.; Rivera, M.; Mcgroarty, E. J. Neutron Scattering Analysis of Bacterial Lipopolysaccharide Phase Structure - changes at high pH. *J. Biol. Chem.* **1987**, *262*, 5100–5105.

(20) Labischinski, H.; Vorgel, E.; Uebach, W.; May, R. P.; Bradaczek, H. Architecture of bacterial lipid A in solution - a neutron small-angle scattering study. *Eur. J. Biochem.* **1990**, *190*, 359–363.

(21) Galanos, C.; Luderitz, O.; Westphal, O. A New Method for the Extraction of R Lipopolysaccharides. *Eur. J. Biochem.* **1969**, *9*, 245–249.

(22) Apicella, M. A. Isolation and characterization of lipopolysaccharides. *Methods Mol. Biol.* **2008**, *431*, 3–13.

(23) Darveau, R. P.; Hancock, R. E. W. Procedure for isolation of bacterial lipopolysaccharides from both smooth and rough Pseudomonas aeruginosa and Salmonella typhimurium strains. *J. Bacteriol.* **1983**, *155*, 831–838.

(24) Lam, N. H.; Ha, B. Y. Surface-Lattice Model Describes Electrostatic Interactions of Ions and Polycations with Bacterial Lipopolysaccharides: Ion Valence and Polycation's Excluded Area. *Langmuir* **2014**, *30*, 13631–40.

(25) Nikaido, H. Molecular Basis of Bacterial Outer Membrane Permeability Revisited. *Microbiol. Mol. Biol. Rev.* **2003**, *67*, 593–656.

(26) Almgren, M.; Edwards, K.; Karlsson, G. Cryo transmission electron microscopy of liposomes and related structures. *Colloids Surf., A* **2000**, *174*, 3–21.

(27) Heenan, R. K.; Penfold, J.; King, S. M. SANS at Pulsed Neutron Sources: Present and Future Prospects. *J. Appl. Crystallogr.* **1997**, *30*, 1140–1147.

(28) Singh, S.; Papareddy, P.; Kalle, M.; Schmidtchen, A.; Malmsten, M. Importance of lipopolysaccharide aggregate disruption for the anti-endotoxic effects of heparin cofactor II peptides. *Biochim. Biophys. Acta* **2013**, *1828*, 2709–2719.

(29) King, S. M. *Modern Techniques for Polymer Characterisation*; J. Wiley, 1999; Chapter 7, Small-Angle Neutron Scattering, pp 171–231.

(30) Pedersen, J. S.; Schurtenberger, P. Scattering Functions of Semiflexible Polymers with and without Excluded Volume Effects. *Macromolecules* **1996**, *29*, 7602–7612.

(31) Ulevitch, R. J.; Johnston, A. R. The modification of biophysical and endotoxic properties of bacterial lipopolysaccharides by serum. *J. Clin. Invest.* **1978**, *62*, 1313–1324.

(32) Aurell, C. A.; Wistrom, A. O. Critical Aggregation Concentrations of Gram-Negative Bacterial Lipopolysaccharides (LPS). *Biochem. Biophys. Res. Commun.* **1998**, *253*, 119–123.

(33) Kotlarchyk, M.; Sheu, E.; Capel, M. Structural and dynamical transformations between neighboring dense microemulsion phases. *Phys. Rev. A: At., Mol., Opt. Phys.* **1992**, *46*, 928–939.

(34) Heenan, R. *"FISH" Data Analysis Program*; Rutherford Appleton Laboratory (RAL) and Science and Engineering Research Council (SERC), Chilton (GB).; Rutherford Appleton Laboratory scientific report, 1989; pp 89–129.

(35) Kholodenko, A. L. Analytical calculation of the scattering function for polymers of arbitrary flexibility using the Dirac propagator. *Macromolecules* **1993**, *26*, 4179–4183.

(36) Domingues, M. M.; Castanho, M. A. R. B.; Santos, N. C. rBPI(21) promotes lipopolysaccharide aggregation and exerts its antimicrobial effects by (hemi)fusion of PG-containing membranes. *PloS one* **2009**, *4*, e8385.

(37) Risco, C.; Carrascosa, J. L.; Bosch, M. A. Visualization of Lipopolysaccharide Aggregates by Freeze-Fracture and Negative Staining. *J. Electron Microsc.* **1993**, *42*, 202–204.

(38) Bergstrand, A.; Svanberg, C.; Langton, M.; Nyden, M. Aggregation behavior and size of lipopolysaccharide from Escherichia coli O55:B5. *Colloids Surf., B* **2006**, *53*, 9–14.

(39) Snyder, S.; Kim, D.; McIntosh, T. J. Lipopolysaccharide Bilayer Structure: Effect of Chemotype, Core Mutations, Divalent Cations, and Temperature. *Biochemistry* **1999**, *38*, 10758–10767.

(40) Neville, F.; Cahuzac, M.; Konovalov, O.; Ishitsuka, Y.; Lee, K. Y. C.; Kuzmenko, I.; Kale, G. M.; Gidalevitz, D. Lipid Headgroup Discrimination by Antimicrobial Peptide LL-37: Insight into Mechanism of Action. *Biophys. J.* **2006**, *90*, 1275–1287.

(41) Lundquist, A.; Wessman, P.; Rennie, A. R.; Edwards, K. Melittin-Lipid interaction: A comparative study using liposomes, micelles and bilayerdisks. *Biochim. Biophys. Acta, Biomembr.* **2008**, *1778*, 2210–2216.

(42) Coughlin, R. T.; Haug, A.; Mcgroarty, E. J. Physical Properties of Defined Lipopolysaccharide Salts. *Biochemistry* **1983**, *22*, 2007–2013.

(43) Richter, W.; Vogel, V.; Howe, J.; Steiniger, F.; Brauser, A.; Koch, M. H.; Roessle, M.; Gutsmann, T.; Garidel, P.; Mantele, W.; Brandenburg, K. Morphology, size distribution, and aggregate structure of lipopolysaccharide and lipid A dispersions from enterobacterial origin. *Innate Immun.* **2011**, *17*, 427–438.

(44) Arseneault, M.; Bédard, S.; Boulet-Audet, M.; Pézolet, M. Study of the Interaction of Lactoferricin B with Phospholipid Monolayers and Bilayers. *Langmuir* **2010**, *26*, 3468–3478.

(45) Ulvatne, H.; Haukland, H.; Olsvik, O.; Vorland, L. Lactoferricin B causes depolarization of the cytoplasmic membrane of Escherichia coli ATCC 25922 and fusion of negatively charged liposomes. *FEBS Lett.* **2001**, *492*, 62–65.

(46) Yeaman, M. R.; Yount, N. Y. Mechanisms of Antimicrobial Peptide Action and Resistance. *Pharmacological Reviews* **2003**, *55*, 27–55.

(47) Yount, N. Y.; Bayer, A. S.; Xiong, Y. Q.; Yeaman, M. R. Advances in antimicrobial peptide immunobiology. *Biopolymers* **2006**, *84*, 435–458.

(48) Chen, X.; Howe, J.; Andrä, J.; Rossle, M.; Richter, W.; da Silva, A. P.; Krensky, A. M.; Clayberger, C.; Brandenburg, K. Biophysical analysis of the interaction of granulysin-derived peptides with enterobacterial endotoxins. *Biochim. Biophys. Acta* **2007**, *1768*, 2421–2431.

(49) Zhang, G.-H.; Mann, D. M.; Tsai, C.-M. Neutralization of Endotoxin In Vitro and In Vivo by a Human Lactoferrin-Derived Peptide. *Infect. Immun.* **1999**, *67*, 1353–1358.

TOC Graphic

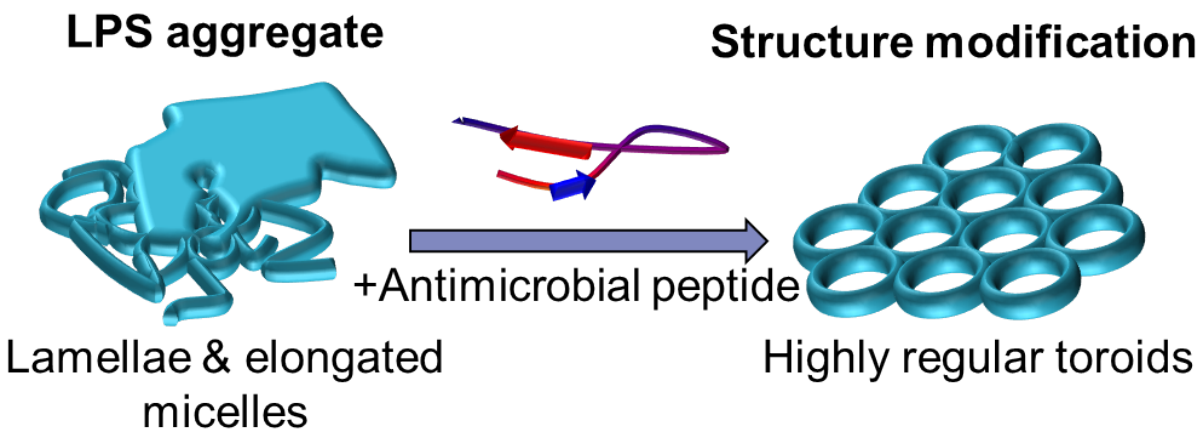

Figure 9: Table of Contents Graphic file *float/TOCgraphic.tif*